

Pulse Echo and Combined Resonance Techniques: A Full Set of LGT Acoustic Wave Constants and Temperature Coefficients

Blake T. Sturtevant, *Student Member, IEEE*, Peter M. Davulis, *Student Member, IEEE*,
and Mauricio Pereira da Cunha, *Senior Member, IEEE*

Abstract—This work reports on the determination of langatate elastic and piezoelectric constants and their associated temperature coefficients employing 2 independent methods, the pulse echo overlap (PEO) and a combined resonance technique (CRT) to measure bulk acoustic wave (BAW) phase velocities. Details on the measurement techniques are provided and discussed, including the analysis of the couplant material in the PEO technique used to couple signal to the sample, which showed to be an order of magnitude more relevant than the experimental errors involved in the data extraction. At room temperature, elastic and piezoelectric constants were extracted by the PEO and the CRT methods and showed results consistent to within a few percent for the elastic constants. Both raw acquired data and optimized constants, based on minimization routines applied to all the modes involved in the measurements, are provided and discussed. Comparison between the elastic constants and their temperature behavior with the literature reveals the recent efforts toward the consistent growth and characterization of LGT, in spite of significant variations (between 1 and 30%) among the constants extracted by different groups at room temperature. The density, dielectric permittivity constants, and respective temperature coefficients used in this work have also been independently determined based on samples from the same crystal boules. The temperature behavior of the BAW modes was extracted using the CRT technique, which has the advantage of not relying on temperature dependent acoustic couplants. Finally, the extracted temperature coefficients for the elastic and piezoelectric constants between room temperature and 120°C are reported and discussed in this work.

I. INTRODUCTION

LANGATATE ($\text{La}_3\text{Ga}_{5.5}\text{Ta}_{0.5}\text{O}_{14}$, LGT), which has the same the point group 32 crystal symmetry as quartz, has been shown to possess piezoelectric coupling constants 3 to 4 times larger than quartz, high density (6147 kg/m³), no crystalline phase change up to its melting point, and experimentally determined temperature compensated orientations [1]–[4]. For these reasons, it has been consid-

ered an attractive acoustic wave (AW) material for frequency control, communications, and sensor applications. To accurately design AW devices, a reliable set of AW constants at a reference temperature (T_0) along with the behavior of these constants in a range of temperatures around T_0 is critical. The room temperature AW constants and temperature coefficients found in the literature show significant discrepancies among themselves regarding the values of some of these constants (for instance, 25% discrepancy is found in the literature for the value of C_{13} at room temperature) [2]–[7]. Moreover, the measured temperature behaviors of bulk acoustic waves (BAW) and surface acoustic waves (SAW) do not match the respective mode predictions using the currently available AW LGT constants and temperature coefficients [2], [8]. These existing discrepancies motivated the present work.

This paper reports on a full set of the LGT material constants and temperature coefficients from 5 to 120°C required for the prediction of AW mode performance along arbitrary orientations. To mitigate systematic errors associated with a single measurement technique, room temperature BAW phase velocities were extracted by 2 independent methods at room temperature: 1) pulse echo overlap (PEO) and 2) a combined resonance technique (CRT), which uses both thickness and laterally excited BAW resonant modes [9]–[12]. The phase velocities of 13 distinct BAW modes were measured at 7 temperature values between 5 and 120°C using the CRT technique.

These BAW measurements, together with the density and the 2 dielectric permittivities (ϵ_{11} , ϵ_{33}) reported in [13], [14], were used to determine the elastic and piezoelectric constants at a reference temperature ($T_0 = 25^\circ\text{C}$). Bulk acoustic wave measurements reported in this work between 5 and 120°C with the thermal expansion coefficients and dielectric temperature coefficients reported in [13], [14] were employed to determine the elastic and piezoelectric temperature coefficients. The measurement of 13 modes for the determination of 8 independent constants (6 elastic and 2 piezoelectric) enabled consistency checks among the extracted values. An optimization routine was implemented to minimize the error in the full set of 13 equations by allowing the preliminary set of constants to vary.

Section II reviews the measurements techniques employed in this work. Section III describes how the AW constants are extracted from full sets of measured BAW velocities for both the PEO and CRT techniques. Section IV discusses the experimental results including the un-

Manuscript received May 21, 2008; accepted December 11, 2008. This project was funded in part by the Army Research Office ARO Grant #DAAD19-03-1-0117, by the Petroleum Research Fund Grant ACS PRF #42747-AC10, by the National Science Foundation grants #ECS 0134335 and #DGE-0504494, and the Air Force Office AFO Grant #FA9550-07-1-0519.

The authors are with the Laboratory for Surface Science & Technology, University of Maine, Orono, ME.

B. T. Sturtevant is also with the Department of Physics, University of Maine, Orono, ME.

P. M. Davulis and M. Pereira da Cunha are both with the Department of Electrical and Computer Engineering, University of Maine, Orono, ME.

Digital Object Identifier 10.1109/TUFFC.2009.1101

certainty associated with the different methods. Finally, Section V concludes the paper.

II. REVIEW OF MEASUREMENT TECHNIQUES

A. Sample Preparation

All samples used in this work were prepared for measurement at University of Maine's Microwave Acoustic Materials Laboratory (MAML) and originated from a commercial LGT boule (FOMOS, Moscow, Russia). An X-ray-diffraction-based procedure for crystal alignment described in [15] was employed initially with a Scintag X3 Advanced Diffraction System (Scintag/Thermo Electron Corporation, Waltham, MA) and later with a PANalytical X'Pert Pro Materials Research Diffractometer (PANalytical Inc., Natick, MA). This technique enabled alignment of the samples to better than $6'$. After alignment, samples were cut with an inner diameter saw (Meyer-Berger, Steffisberg, Switzerland), ground, and polished to an optical finish.

Two types of samples were prepared: parallelepipeds for the PEO experiments and wafers for the CRT and dielectric experiments. The PEO parallelepipeds were of 2 kinds: 1) the first had faces normal to the X, Y, Z crystallographic axes customarily used for quartz and other point group 32 crystals and had dimensions of 15.0 mm, 20.7 mm, 21.6 mm (X, Y, Z); 2) the other had faces normal to $Y \pm 45^\circ$ (third face normal to X) and dimensions of 21.7 mm, 21.8 mm, and 15.5 mm ($Y+45^\circ$, $Y-45^\circ$, X) and was used for the measurement of the Y-rotated modes. The dimensions of these parallelepipeds were calculated to minimize spurious reflections that result from mode conversion and the respective power flow angles of the different modes in the anisotropic crystal [16].

Five types of plates, with the larger faces normal to the X, Y, Z, and $Y \pm 45^\circ$, were prepared with thicknesses between 400 and 700 μm for the CRT measurements. This range of wafer thicknesses was selected as a compromise between the appropriate excitation of the resonant BAW modes of interest and acceptable relative uncertainty for the thickness measurements. The dimensions of both the plates and parallelepipeds were determined through 5-point measurements using a precision length gauge (Heidenhain Corporation, Schaumburg, IL). Looking down at the sample, one measurement point was taken in the center of the sample and 4 measurements were made around the perimeter of the sample. The linear dimension used in the determination of BAW phase velocity was taken as the average of these 5 points.

B. Pulse Echo Overlap (PEO)

The conventional pulse echo technique as described in [9], [10] is used here with the addition of a couplant correction reported in [17]. The couplant correction, detailed in the appendix, accounts for the phase shift introduced

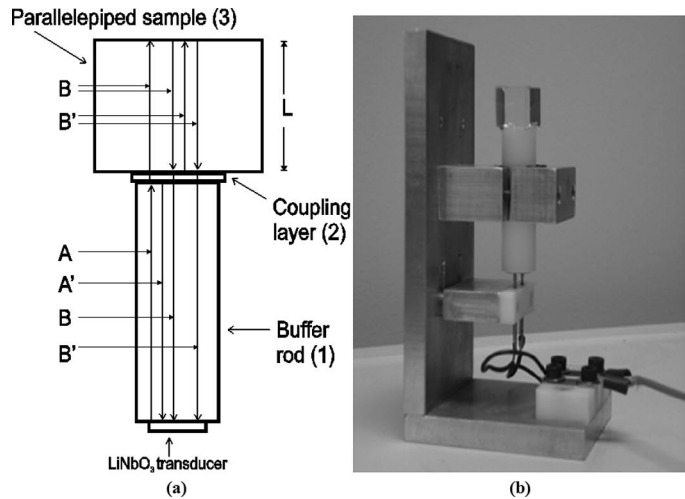


Fig. 1. (a) Schematic of the PEO test fixture and (b) transducer, buffer rod, and sample mounted in the test fixture. The input signal from the generator is transmitted to the transducer via pogo pins.

to the AWs by the acoustic coupling agent at the buffer rod/sample interface.

As depicted in Fig. 1(a), LiNbO₃ transducers with fundamental resonant modes around 6 MHz were used to introduce AWs to a buffer rod that travel to the sample. A 36° Y-rotated cut LiNbO₃ transducer was used to excite the longitudinal modes and a 163° Y-rotated cut LiNbO₃ was used to excite the shear modes. Each transducer had a diameter of 12.0 mm and an active area 7.0 mm in diameter. The transducers were attached to a fused silica buffer rod that was 50 mm in length and 15.0 mm in diameter, using a 99.99% pure indium foil (Indium Corporation, Utica, NY) and were kept connected to the buffer rod for multiple tests. With the exception of the degenerate shear mode along the crystalline Z axis, there are 3 unique BAW modes measurable along the 5 directions chosen for this study; thus, 14 modes were measurable by PEO.

The transducer, buffer rod, and sample, shown mounted in a test fixture in Fig. 1(b), were placed inside an oven and maintained at 25°C ($\pm 0.5^\circ\text{C}$). A RITEC RAM-5000 pulse generator (Ritec Inc., Warwick, RI) was used to excite the transducers. Waveforms of the initial pulse and subsequent reflections were digitized and recorded using a LeCroy Wavepro 7100 oscilloscope (LeCroy Corporation, Chestnut Ridge, NY). For the determination of the time difference between 2 pulses, $\Delta t'$, a high-resolution waveform (0.2 ns/data point) was recorded, loaded into Matlab (MathWorks, Natick, MA), and plotted on top of a copy of itself. A time offset, $\Delta t''$, was added to one of the 2 waveforms until the 2 pulses of interest overlap each other. Fig. 2 exemplifies the procedure described with a typical measured waveform as captured from the oscilloscope, Fig. 2(a), and the superposition of 2 pulses after the addition of the time delay, Fig. 2(b).

C. Combined Resonance Technique (CRT)

The CRT used nonmetallized wafers for both lateral field excitation (LFE) and thickness field excitation

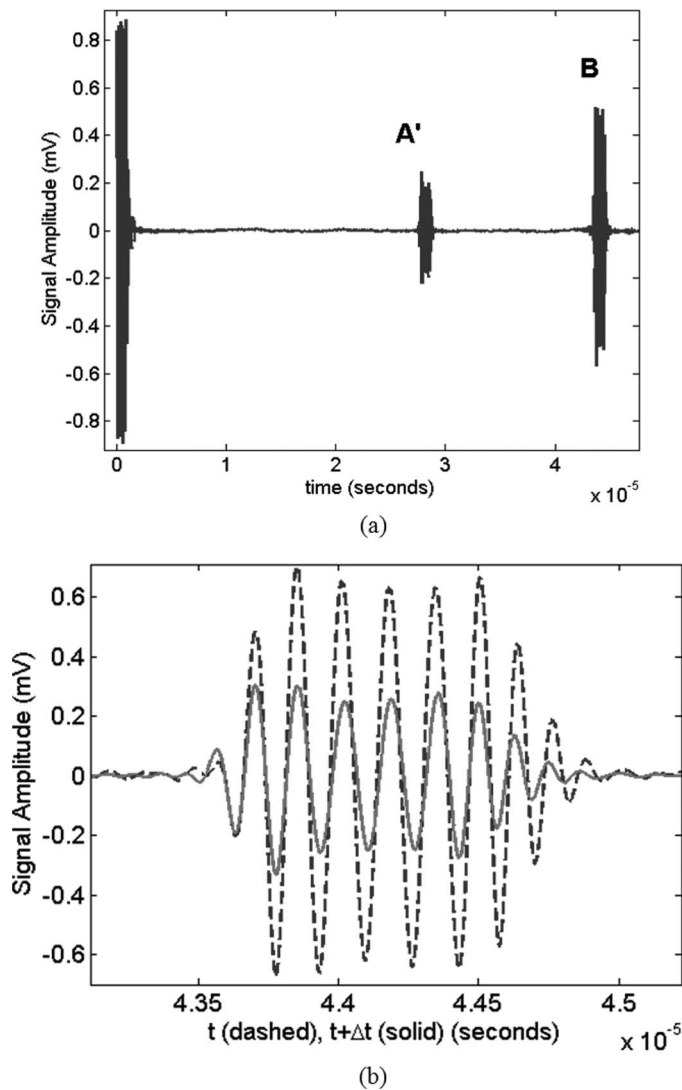


Fig. 2. (a) Waveform including initial pulse from the generator and the reflected signals A' and B; (b) overlap of 2 pulses of interest: the solid line is the reflection from the buffer rod, signal A', and the dashed line is the reflection from the back face of the parallelepiped sample, B.

(TFE) resonator measurements to minimize nonuniform distribution of motion (NUDM) effects [11], [12], which have been shown to lead to measurable discrepancies in the extracted piezoelectric constants [11]. In addition, the CRT lends itself nicely to measurements at different temperatures because there is no metallization or acoustic coupling agent whose properties change with temperature. The frequencies of interest in these measurements, which do not depend on NUDM effects, are the LFE resonant (f_R) and TFE antiresonant (f_{AR}), which are related to the BAW phase velocity, v_p , by the wave relationship, $f_{AR/R} \times \lambda = v_p$, where $\lambda = 2 \times (\text{wafer thickness})/n$ for the n th harmonic.

The fabricated LFE test fixture consists of semicircular electrodes etched on a circuit board atop which the sample sits, as shown in Fig. 3(a). The TFE test fixture, shown in Fig. 3(b), consists of 2 modified General Radio 874 open circuit loads with custom machined parts.

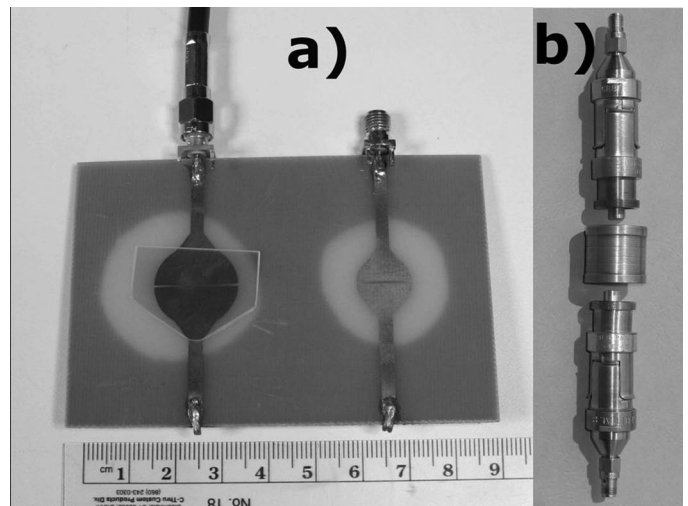


Fig. 3. Combined resonance technique measurement fixtures: a) lateral field excitation and b) thickness field excitation.

The relative separation of the electrodes is changed by screwing or unscrewing the connectors. The LFE resonant and TFE antiresonant frequencies were measured using an Agilent 4396B network analyzer configured with an 85046A S-parameter test set (Agilent Technologies, Inc., Palo Alto, CA).

Thirteen BAW modes were measured using 5 LGT plates oriented along crystalline axes X, Y, Z, and $\pm 45^\circ$ Y-rotated cuts. One less mode than the PEO method was measurable, because CRT does not allow for the electrical excitation of the Z-longitudinal BAW mode. For each mode, all identifiable harmonics were recorded. The normalized frequencies ($f_{AR/R}/n$) for all measured harmonics were compared, and an average of those that converged was taken as the $f_{AR/R}$ for each particular mode, as described in [11], [12]. These frequencies, along with the measured thickness of the wafers, were used to determine the BAW plane wave velocities through the wave relationship.

D. Dielectric Permittivity Measurements

The dielectric permittivity constants of LGT, ϵ_{11} and ϵ_{33} , were extracted from capacitance measurements using a conducting nickel spray for the electrode deposition [14]. LGT wafers were fabricated with faces normal to the X, Y, and Z axes. The data from the X and Y plates were averaged together to determine ϵ_{11} . Several different capacitors were created with a ground electrode covering one surface of an LGT wafer and a round electrode on the other face. The capacitors were made with circular electrodes of different radii to quantify the relationship between circumference and fringing capacitance, as described in [18]. The capacitances were measured with a Precision LCR Meter (Agilent 4284A, Santa Clara, CA) at a frequency of 10 kHz. The data from the different capacitors were plotted and a best-fit line was obtained using a total least squares algorithm [19], from which the relative dielectric permittivity was extracted. Each of the

TABLE I. METHOD OF ELASTIC AND PIEZOELECTRIC CONSTANT EXTRACTION FOR A CLASS 32 CRYSTAL.

Constants (in order of extraction)	Method of extraction (modes and other constants used)
C_{44}	ZS
C_{66}	XFS & XSS using C_{44}
C_{11}	YL & YFS using C_{44}
e_{11}	XL using C_{11} & ϵ_{11}
	YSS using C_{66} & ϵ_{11}
C_{14}	XFS & XSS using C_{44} & C_{66}
	YL & YFS using C_{11} & C_{44}
	ZL
C_{33}	Y-45L & Y-45FS using C_{11} , C_{44} , C_{14}
	Y+45L & Y+45SS using C_{11} , C_{44} , C_{14}
C_{13}	Y-45L & Y-45FS using C_{11} , C_{44} , C_{14} , C_{33}
	Y+45L & Y+45SS using C_{11} , C_{44} , C_{14} , C_{33}
e_{14}	Y+45FS using C_{14} , C_{44} , C_{66} , ϵ_{11} , ϵ_{33} , e_{11}
	Y-45SS using C_{14} , C_{44} , C_{66} , ϵ_{11} , ϵ_{33} , e_{11}

Nomenclature used for modes: the first letter indicates direction of propagation (X, Y, Z, Y+45°, Y-45°) and the second and third letters indicate mode (L: longitudinal or quasi-longitudinal; FS: fast-shear or quasi-fast-shear; SS: slow-shear or quasi-slow-shear). Along Z, only one unique shear mode, ZS, exists.

capacitors was tested at 11 temperatures, ranging from 25° to 120°C, and the data were used to find the dielectric constants at each of the temperatures. The Taylor series temperature coefficients were fitted to the dielectric data.

III. EXTRACTION TECHNIQUE

A. Extraction of Room Temperature Constants

The phase velocity values of 14 BAW modes for PEO and 13 BAW modes for CRT, along with values for the LGT density, 6147.7 kg/m³ [13], and dielectric constants [14], were used to determine an initial set of best-guess values for the elastic and piezoelectric constants. Table I outlines the process by which the phase velocities were combined to calculate the elastic and piezoelectric constants. The BAW phase velocities nomenclature used in Table I is as follows: X, Y, Z, and Y ± 45° denote the direction of wave propagation; L, FS, and SS describe the mode of propagation (longitudinal or quasi-longitudinal, fast-shear or quasi-fast shear, and slow-shear or quasi-slow-shear, respectively). Because the Z-longitudinal mode is not excitable using CRT, the extraction of C_{33} directly from the ZL mode could only be accomplished by the PEO technique.

As noted in Table I, many of the constants can be extracted and, in fact, were extracted through different combinations of modes, according to the procedure outlined in [12]. The values of the constants extracted through different combinations of velocities listed in Table I were checked for consistency, and an optimization technique was conducted to refine the extracted values of the elastic and piezoelectric constants. This optimization technique relied on the minimization of the norm between the measured

BAW phase velocities and the BAW phase velocities calculated using the extracted constants. The constants were allowed to vary within bounded limits using an iterative search. The search procedure avoided accepting results that included the constant values at the boundaries of the search, because those often do not represent minima for the optimization function. If the search selected constants lying on a boundary, the bounds were slightly extended until a full set of constants was found within the limits, as given in the following section.

B. Extraction of Temperature Coefficients

Phase velocities were measured at 7 temperatures between 5 and 120°C using the CRT technique. At each measured temperature, a set of elastic and piezoelectric constants was determined by the procedure described in Sections II and III-A. Each constant was then plotted versus temperature and the temperature coefficients, TC1 and TC2, were extracted from a second order polynomial fit to the measured data. The value of a material constant, X_{ij} (either C_{ij} or e_{ij}), at a temperature, T , is then expressed by the expansion:

$$X_{ij}(T) = X_{ij}(25) \times (1 + \text{TC1} \times (T - 25) + \text{TC2} \times (T - 25)^2). \quad (1)$$

IV. EXPERIMENTAL RESULTS

A. PEO Couplant Correction

The fundamental uncertainties in the phase velocity are attributable to the relative uncertainty in the measurement of the sample dimensions and in the measurement of the time of flight. The former, as indicated in Section II-A, is $\sim 10^{-4}$ and the latter is at least an order of magnitude smaller. More importantly, due to the mismatch of the acoustic impedances of the couplant with the sample and buffer rod as well as the finite thickness of the couplant, the couplant correction accounted for a 10^{-3} variation in the phase velocities, greater than the 10^{-4} uncertainties in sample dimension measurements, indicating that the couplant effect should be taken into account. Early experiments with quartz samples were used to validate the PEO technique employed. These measurements and the resulting calculated constants were compared with well-known quartz constants [20] and showed that the maximum discrepancy between calculated and measured values dropped from 0.9% to 0.6% once the effect of the couplant used to bond the sample to the buffer rod was included in the analysis.

B. Room Temperature Measurements

Table II presents the LGT BAW velocities measured by PEO before and after considering the couplant correction (phase velocity no couplant correction, PvNC, and phase

TABLE II. BULK ACOUSTIC WAVE VELOCITIES IN LGT.

Mode	PvNC [m/s]	PvC [m/s]	$\Delta_C \cdot 10^4$	$\Delta_{rel} \cdot 10^4$
XL	5576.2	5576.2	0.0	1.53
XFS	3135.3	3138.3	9.7	1.53
XSS	2249.2	2251.5	10.2	1.53
YL	5561.3	5556.5	-8.6	0.73
YFS	2845.3	2847.0	6.0	0.73
YSS	2604.4	2608.7	6.5	0.73
ZL	6527.1	6527.1	0.0	1.25
ZS	2882.2	2884.0	6.2	1.25
Y+45L	5775.6	5776	0.7	1.71
Y+45FS	3110.4	3109.7	-2.3	1.71
Y+45SS	3081.5	3083.5	6.5	1.71
Y-45L	6099.0	6104.9	9.7	0.92
Y-45FS	3168.1	3169.5	4.4	0.92
Y-45SS	2289.1	2290.7	7.0	0.92

$\Delta_C = (PvC - PvNC)/PvC$, where PvC are the phase velocities with couplant correction, and PvNC are the phase velocities with no couplant correction.

Δ_{rel} is the relative uncertainty in the velocity measurements, as discussed in the text.

velocity with couplant correction, PvC, respectively). Also included in Table II are the corrections introduced by considering the couplant, $\Delta_C = (PvC - PvNC)/PvC$, and the relative fundamental uncertainty in the phase velocity, $\Delta_{rel} = \sqrt{[(-l/t^2) \times \Delta t]^2 + [(1/t) \times \Delta l]^2} \times (t/l)$, which is dominated by the uncertainty in sample dimensions. In the expression for Δ_{rel} , l is the path length traveled by the AW, t is the time of flight, Δl and Δt represent the fundamental experimental uncertainties in the respective quantities. As can be seen from Table II, the effect of considering the couplant accounts for a phase velocity correction around 3.5 times larger than the relative uncertainty in the phase velocity measurements on the average for all modes, and up to an order of magnitude larger for several of the modes measured.

Regarding the CRT measurements, the odd numbered resonant frequencies were measured, normalized, and compared with determine $f_{AR/R}$ for each BAW mode. Depending on the orientation, the measurable harmonics obtained with the plano-plano plates prepared varied between $n = 1$ to $n = 5$ (for example, Y-45 FS mode) and $n = 1$ to $n = 19$ (for example, Y-45 L mode). The odd harmonics between $n = 1$ and $n = 11$ were typically measured. The fundamental and higher harmonic resonant frequencies were normalized by dividing them by their respective harmonic number. The normalized frequencies were averaged for each mode to determine an $f_{AR/R}$ for calculation of the BAW phase velocity. Prior to averaging, resonant peaks that showed a significant discrepancy with respect to random variations were discarded as outliers. The fundamental was found to be an outlier for 10 of the 13 modes, which is consistent with other reported CRT data [11], [12]. For this reason, the fundamental was consistently not used in the $f_{AR/R}$ averaging calculation. Typically, the normalized odd harmonics 3 through 11 were used to determine $f_{AR/R}$.

TABLE III. MEASURED VELOCITY COMPARISON.

Propagation Direction and Mode	Measured Velocities (25°C)		
	V_{CRT}	V_{PEO}	% Diff.*
X			
L	5563.9	5576.2	0.22%
FS	3136.0	3138.5	0.08%
SS	2244.5	2251.5	0.31%
Y			
L	5508.0	5556.5	0.88%
FS	2816.5	2847.0	1.08%
SS	2591.1	2608.7	0.68%
Z			
L	NM	6527.1	—
S	2884.2	2884.0	-0.01%
Y+45			
L	5809.2	5776.0	-0.57%
FS	3088.2	3109.7	0.69%
SS	3054.3	3083.5	0.95%
Y-45			
L	6068.4	6104.9	0.60%
FS	3157.1	3169.5	0.39%
SS	2285.5	2290.7	0.23%

*% Difference = $(V_{PEO} - V_{CRT})/V_{PEO} \times 100\%$.

NM = Not measurable.

The room temperature phase velocity measurements based on the PEO (after couplant correction) and the CRT are compared in Table III. The agreement between the BAW phase velocities measured through the CRT and couplant corrected PEO is 11 parts in a thousand in the worst case and about 5 parts in a thousand when all modes are averaged. The accuracy of the phase velocities determined with the CRT technique, as in the PEO case, was limited by the plate thickness measurement uncertainties. The relative uncertainty of the resonant plate thickness measurements was better than 5×10^{-3} .

Table IV shows the values of the room temperature coefficients determined by PEO and CRT before and after the optimization routine. For constants obtained from Table I using a single method of extraction (i.e., C_{33} for PEO, C_{44} , C_{11} , C_{66}), the uncertainty was calculated by propagating the experimental uncertainty in the phase velocity measurements (dominated by the uncertainty in the sample dimensions, as previously discussed) through the algebraic equations relating the constant values and velocities [12] and is relatively small. For constants obtained from Table I through more than one method of extraction, (i.e., C_{12} , C_{13} , C_{14} , and e_{14}), the value for the constant was taken as the average of the constant values found from the different methods and the uncertainty taken as the standard deviation in these constant values. As a result, the estimated uncertainty for these constants was higher. It can also be observed from Table IV that the optimization routine results in values for the elastic constants determined by PEO that differ from 0.1 to 4% when compared with the constants before optimization. As shown in the table, the variations introduced to the constants determined through PEO by the optimization routine are about 25 times higher on average than the calculated experimental uncertainties. This result indicates that there

TABLE IV. ROOM TEMPERATURE CONSTANTS BEFORE AND AFTER NUMERICAL OPTIMIZATION.

	V_{PEO}			V_{CRT}			$V_{\text{PEO}}, V_{\text{CRT}}\%$ Diff.*
	Before optim.	After optim.	% Change	Before optim.	After optim.	% Change	
C_{ij}^E (GPa)							
C_{11}^E	188.47 ± 0.04	189.41	0.5%	184.10	188.54	2.4%	-0.5%
C_{12}^E	107.31 ± 0.1	109.06	1.6%	103.53	108.98	5.3%	-0.1%
C_{13}^E	104.87 ± 0.8	100.63	4.0%	108.97	100.43	-7.8%	-0.2%
C_{14}^E	13.61 ± 0.1	13.60	0.1%	13.71	13.13	-4.2%	-3.5%
C_{33}^E	263.61 ± 0.07	262.29	0.5%	267.30	264.63	-1.0%	0.9%
C_{44}^E	50.12 ± 0.01	51.12	1.0%	51.13	50.49	-1.2%	-1.2%
C_{66}^E	40.57 ± 0.03	40.17	1.0%	40.28	39.78	-1.3%	-1.0%
e_{ij} (C/m ²)							
e_{11}	-0.556 ± 0.2	-0.518	6.8%	-0.705	-0.482	-31.6%	-7.2%
e_{14}	0.336 ± 0.278	0.051	84.8%	-0.582	0.167	-128.8%	106%

*% Difference = $(V_{\text{CRT}} - V_{\text{PEO}})/\text{Average} \times 100\%$, where Average = $(V_{\text{CRT}} + V_{\text{PEO}})/2$, with the values for V_{CRT} and V_{PEO} taken after optimization.

TABLE V. ELASTIC AND PIEZOELECTRIC CONSTANTS (25°C).

	This Work	[2]	[3]	[4]	[5]	[6]
C_{ij}^E (GPa)						
C_{11}^E	189.41	188.60	189.40	188.90	202.00	188.81
C_{12}^E	109.06	107.90	108.40	108.60	120.00	107.84
C_{13}^E	100.63	103.40	132.00	104.40	125.00	100.15
C_{14}^E	13.60	13.50	13.70	13.74	13.30	13.50
C_{33}^E	262.29	261.90	262.90	264.50	288.00	261.05
C_{44}^E	51.12	51.10	51.25	51.29	49.70	50.95
C_{66}^E	40.17	40.30	40.52	40.19	40.70	40.49
e_{ij} (C/m ²)						
e_{11}	-0.518	-0.456	-0.54	0.508	-0.468	-0.478
e_{14}	0.051	0.094	0.07	-0.028	0.0632	0.043
$\varepsilon_{ij}^S/\varepsilon_o$						
$\varepsilon_{11}^S/\varepsilon_o$	17.69	18.3	18.5	19.6	19.3	19.1
$\varepsilon_{33}^S/\varepsilon_o$	70.73	78.9	60.9	76.5	80.3	77.2

are unidentified sources of error, which may include effects of sample preparation, such as alignment, parallelism, and plate shape, and possibly deviations from perfect crystallinity or imperfect homogeneity throughout the crystal.

Table IV also shows the values of the room temperature coefficients determined by PEO and CRT after the optimization routine described in Section III-A, independently applied to both techniques. The final set of constants found through the optimization procedure decreased the norm of the difference vector by 84% for the PEO data and 71% for the CRT data. The optimized constants for PEO and CRT in Table IV agree well, with the largest difference in elastic constants being 3.5% for C_{13} . The large difference between the values for e_{14} extracted by PEO and CRT reflects the reduced influence that this constant has in the BAW modes measured and thus the difficulty in extracting it through the methods described. Because the absolute norm of the difference vector was 4 times lower for the PEO data than for the CRT data, the constants extracted by the PEO measurements were adopted as the room temperature constants.

Table V compares the optimized PEO constants at room temperature with those published in the literature. As can be seen from this table, C_{13} values in the literature fall into 2 different ranges: one around 102 GPa, the

other close to 127 GPa. Our determined value for C_{13} , 100.63 GPa, falls in the first group. The use of different dielectric constants can influence the determination of the elastic and piezoelectric constants from measured BAW phase velocities. For instance, the variation of ε_{33} by up to 13% in Table V can partially account for the discrepancy in piezoelectric constants, but cannot directly account for all of the variations in the elastic constants. It is not clear at this point if the existing discrepancies for the acoustic wave constants are due to potential variations in either the chemical homogeneity or thermal history [21], [22] of crystals originating from different suppliers or to different measurement techniques and data processing by different groups or, more likely, to a combination of both factors.

In this work, the use of multiple modes for the determination of each constant and the minimization of the norm of the difference vector previously discussed proved to be critical in obtaining a consistent set of material constants. This procedure accounts for the fact that there are BAW modes that are more sensitive to changes in a particular constant value than others, as detailed in [23]. For instance, a nearly 200% difference in e_{11} changes the YSS mode by 15% but changes the Y+45FS mode by a mere 1%. These results reflect the importance of using multiple modes for the determination of each constant and the ne-

TABLE VI. EXTRACTED TEMPERATURE COEFFICIENTS ($T_{\text{REF}} = 25^\circ\text{C}$).

	This Work		[2]		[5]	
	TC1 ($10^{-6} \text{ }^\circ\text{C}^{-1}$)	TC2 ($10^{-9} \text{ }^\circ\text{C}^{-2}$)	TC1 ($10^{-6} \text{ }^\circ\text{C}^{-1}$)	TC2 ($10^{-9} \text{ }^\circ\text{C}^{-2}$)	TC1 ($10^{-6} \text{ }^\circ\text{C}^{-1}$)	TC2 ($10^{-9} \text{ }^\circ\text{C}^{-2}$)
C_{11}^E	-71.2	-96.1	-82.31	-444.98	-71.0	-391
C_{12}^E	-138.4	-50.6			-137	-614
C_{13}^E	83.8	-1045.1	-88.63	-415.72	-26.3	47.6
C_{14}^E	-362.1	48.7	-444.28	-243.81	-390	378
C_{33}^E	-85.1	12.5	-101.50	-237.52	-74.1	3.77
C_{44}^E	-1.0	-55.9	21.64	-11.99	-16.1	-133
C_{66}^E	15.1	-154.4	30.35	-450.94	25.6	-64.6
e_{11}	-33.6	969.9	-22.8	-981.00	-42.6	1750
e_{14}	-32.2	-32014.1	-1587.00	2293.00	-135	3530

cessity of minimizing the norm of the difference vector previously defined for overall consistency in the process of extracting the AW constants. The agreement between the room temperature constants determined in this work with a set of constants extracted by resonant ultrasound spectroscopy [6], a method that simultaneously measures nearly 100 resonance peaks in determining the constants, further reinforces the need for calculating constants from over-determined sets of data.

C. Temperature Coefficients

The PEO experiments performed in this work with different acoustic couplants indicated that changing the experimental temperature by more than a few tens of degrees Celsius resulted in variations in the properties of the acoustic couplant with temperature that compromised or obscured any variations in the crystal properties with temperature. The CRT experiments, on the other hand, did not have any coupling or material deposited on the wafers being tested. As a result, the CRT was used for extracting the temperature coefficients. Noting that the temperature coefficients represent changes normalized to a value at a particular reference temperature, the extraction of these coefficients from the CRT data was consistent with the use of PEO values at room temperature.

The temperature coefficients for the elastic and piezoelectric constants extracted according to the procedure in Section III are presented in Table VI. As can be observed from this table, C_{44} and C_{66} exhibit the lowest sensitivity to temperature changes compared with the other constants. This is similar to the case with other crystals of this symmetry class, such as quartz and gallium orthophosphate. The variation of C_{44} to first order, for instance, represents a decrease by about one part in a million per degree Celsius, which is almost 2 orders of magnitude lower than the C_{13} and C_{33} variations with temperature. Table VI also compares the temperature coefficients determined in this work with those of [2] and [5]. The elastic constants C_{11} , C_{44} , and C_{66} and the piezoelectric constant e_{14} have been identified in this work to be less sensitive to temperature changes than other authors have reported. Fig. 4 compares the temperature behavior of selected material constants, normalized to their respective room temperature values, with those reported in [2], [5], and [7] up to 120°C . The

temperature behavior of e_{11} is seen in Fig. 4(a) to vary with temperature in a manner similar to that reported in [5], and almost completely opposite to that reported in [2], [7]. Fig. 4(b) plots the temperature behavior for C_{11} , showing that it is slightly less responsive to temperature changes than has been reported by other authors. Although the overall agreement for $C_{11}(T)$ is quite good up to about 60°C , the variation rises to about 0.4% at 120°C as a result of a similar linear response and a significantly reduced quadratic response reported in this work. Fig. 4(c) compares the effect of temperature on C_{13} . There is a marked difference between the behaviors reported in this work and [5] with respect to the reported in [2] and [7]. In particular, the first-order temperature coefficient observed for this constant is significantly different than as reported in [5], yet leads to a similar value of C_{13} at 120°C due to its strong quadratic component of the temperature behavior. Finally, Fig. 4(d) shows the relative insensitivity of C_{44} to temperature variations. The measured behavior of C_{44} in this work shows temperature changes opposite to that reported in [2] and [7], and also less sensitive than that in [5].

V. CONCLUSIONS

This work has reported on the determination of room temperature elastic and piezoelectric constants for langatate, along with temperature coefficients extracted from measurements performed between 5 and 120°C . Two different techniques, the pulse echo overlap and a combined thickness and lateral field excitation resonance technique, were used in this work to investigate and mitigate a possible bias coming from the use of a single technique. The couplant correction used in the pulse echo overlap measurements is described in detail along with the method used to extract the elastic and piezoelectric constants from phase velocity measurements.

The BAW phase velocity measurements and the elastic constants extracted with the PEO and CRT techniques used in this work agree to better than a few percent. Room temperature constants were finally selected from the PEO technique because of the lower difference norm of these measurements, while temperature behavior was extracted from the CRT, which proved to perform better under

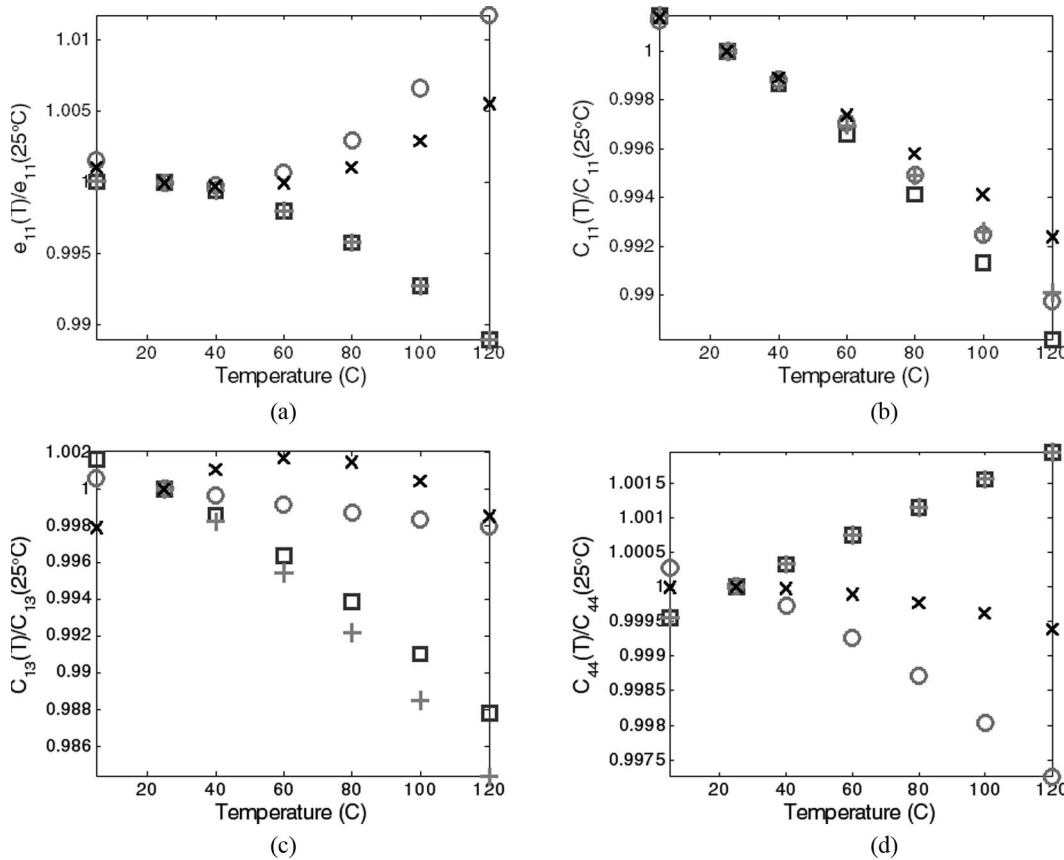


Fig. 4. Constants normalized to their respective values at room temperature and plotted vs temperature for this work and other works reporting temperature coefficients: (a) piezoelectric constant e_{11} , (b) elastic constant C_{11} , (c) elastic constant C_{13} , and (d) elastic constant C_{44} . Symbols used in plots correspond to the following works: \circ = [5], \square = [2], $+$ = [7], and \times = this work.

changing temperature conditions. The room temperature constants obtained in this work were compared with results available in the literature, and maximum discrepancies from a few percent to 31% have been identified for the elastic constants. The first- and second-order temperature coefficients obtained from the CRT measurements and reported in this work were compared with data available in the literature, together with plots for the combined influence of the linear and quadratic temperature coefficients for selected constants. Although one can claim that to a large extent the values obtained are consistent with the literature, reflecting the maturity of LGT as an acoustic wave material, the significant differences reported in this paper indicate the importance of calculating individual constants through multiple modes and techniques as well as minimizing the norm of the difference vector to determine the most consistent set of AW constants.

APPENDIX

As indicated in Section IV, the couplant used to attach the buffer rod to the sample influences the delay between 2 echoes in PEO measurements. The couplant causes a variation in the time delay that is an order of magnitude greater than the experimental uncertainty in these mea-

surements, and thus it must be considered. In this work, the reflection and transmission coefficient phases due to the couplant are calculated by solving for the acoustic impedance in the sample, rather than assuming that this quantity is known, as done in [24], [25], where the need for a couplant correction was discussed.

The first instance where a correction is necessary is in the measurement of the single transit time in the sample, Δt , when the signal A' in Fig. 1(a) is compared with the signal B coming from the back of sample. In this case, the couplant effect is considered through 2 phase shift quantities: Φ_{R13} , which is the added phase shift from A reflecting off the buffer rod/couplant/sample interface; and Φ_{W31} , which is the phase due to the signal A or signal B being transmitted through the sample/couplant/rod interface. The actual transit time in the sample, Δt , is then determined from the measured delay, $\Delta t'$, by

$$\Delta t' = \Delta t + \frac{1}{2\pi f} (2\Phi_{W31} + \Phi_{R13}), \quad (2)$$

where f is the carrier frequency of the tone burst.

Another instance where a correction has to be applied is in the sample delay measurement extracted from a double transit signal in the sample and compared with the single transit signal in the sample; Fig. 1(a), signals B and B'. The delay in the sample is determined in this case by

$$\Delta t' = \Delta t + \frac{\Phi_{R31}}{2\pi f}. \quad (3)$$

The values of the acoustic impedances, $r_j = v_{p,j} \times \rho_j$, for the buffer rod (r_1) and the couplant (r_2) are $r_1 = 1.265 \times 10^7$ kg/m²s and $r_2 = 2.42 \times 10^6$ kg/m²s for the longitudinal modes, and $r_1 = 8.305 \times 10^6$ kg/m²s and $r_2 = 4 \times 10^6$ kg/m²s for the shear modes. The r_1 were obtained from the fused silica buffer rod vendor's specifications [26] while the r_2 values were estimated through preliminary experiments with quartz samples whose r_3 were well known [20]. Expressions for Φ_{W31} , Φ_{R13} , and Φ_{R31} can be derived using a scalar model as in [24], [25] and are found to be

$$\Phi_{W13} = \Phi_{W31} = \tan^{-1} \left[\frac{-d_2 s}{d_1 s} \right] \quad (4)$$

$$\Phi_{R13} = \tan^{-1} \left[\frac{n_2 d_1 c s - n_1 d_2 c s}{n_1 d_1 c^2 + n_2 d_2 s^2} \right] \quad (5)$$

$$\Phi_{R31} = \tan^{-1} \left[\frac{n_2 d_1 c s + n_1 d_2 c s}{-n_1 d_1 c^2 + n_2 d_2 s^2} \right] \quad (6)$$

where the n_i and d_i are defined in terms of the acoustic impedances, r_j , by $n_1 = r_2 r_3 - r_1 r_2$, $n_2 = r_2^2 - r_1 r_3$, $d_1 = r_2 r_3 + r_1 r_2$, $d_2 = r_2^2 + r_1 r_3$, and $c = \cos[k_2 l]$,

$$s = \sin[k_2 l] = \left[\frac{a - (r_2^2 r_3^2 + r_2^2 r_1^2)}{r_2^4 + r_1^2 r_3^2 - r_2^2 r_3^2 - r_2^2 r_1^2} \right]^{1/2}$$

with $a = 2r_1 r_2^2 r_3 (1 + |R_{13}|^2) / (1 - |R_{13}|^2)$.

Using (4) to (6), (2) and (3) can be rewritten solely in terms of the r_j values (note that $\Delta t = \Delta l \times \rho_3 / r_3$ where Δl is the length of the path traveled in the sample) and $|R_{13}|$. $|R_{13}|$ is the modulus of the reflection coefficient for an AW incident on the buffer rod/couplant/sample boundary and can be measured directly by comparing waves reflecting off the end of the buffer rod before and after a sample is mounted. Eq. (2) or (3) is then solved numerically for r_3 from which the phase velocity of the wave in the sample is determined.

ACKNOWLEDGMENT

The authors would like express their gratitude to the personnel from the Laboratory of Surface Science and Technology (LASST) and Department of Electrical and Computer Engineering for valuable technical discussion and for cutting and polishing most of the samples used in this work.

REFERENCES

[1] B. Chai, J. L. Lefaucheur, Y. Y. Ji, and H. Qiu, "Growth and evaluation of large size LGS (La₃Ga₅SiO₁₄), LGN (La₃Ga_{5.5}Nb_{0.5}O₁₄) &

LGT (La₃Ga_{5.5}Ta_{0.5}O₁₄) single crystals," in *Proc. 1998 IEEE Int. Frequency Control Symp.*, pp. 748–760.

[2] M. Pereira da Cunha, D. C. Malocha, E. L. Adler, and K. J. Casey, "Surface and pseudo surface acoustic waves in langatate: Predictions and measurements," *IEEE Trans. Ultrason. Ferroelectr. Freq. Control*, vol. 49, pp. 1291–1299, Sep. 2002.

[3] Y. V. Pisarevsky, P. A. Senyushenkov, B. V. Mill, and N. A. Moiseeva, "Elastic, piezoelectric, dielectric properties of La₃Ga_{5.5}Ta_{0.5}O₁₄ single crystals," in *Proc. 1998 IEEE Int. Frequency Control Symp.*, pp. 742–747.

[4] J. Bohm, E. Chilla, C. Flannery, H.-J. Fröhlich, T. Hauke, R. B. Heilmann, M. Hengst, and U. Straube, "Czochralski growth and characterization of piezoelectric single crystals with langasite structure: La₃Ga₅SiO₁₄ (LGS), La₃Ga_{5.5}Nb_{0.5}O₁₄ (LGN) and La₃Ga_{5.5}Ta_{0.5}O₁₄ (LGT) II. Piezoelectric and elastic properties," *J. Cryst. Growth*, vol. 216, pp. 293–298, Jul. 2000.

[5] N. Onozato, M. Adachi, and T. Karaki, "Surface acoustic wave properties of La₃Ta_{0.5}Ga_{5.5}O₁₄ single crystals," *Jpn. J. Appl. Phys.*, vol. 39, pp. 3028–3031, May 2000.

[6] J. Schreuer, "Elastic and piezoelectric properties of La₃Ga₅SiO₁₄ and La₃Ga_{5.5}Ta_{0.5}O₁₄: An application of resonant ultrasound spectroscopy," *IEEE Trans. Ultrason. Ferroelectr. Freq. Control*, vol. 49, pp. 1474–1479, Nov. 2002.

[7] D. C. Malocha, M. Pereira da Cunha, E. Adler, R. C. Smythe, S. Frederick, M. Chou, R. Helmbold, and Y. S. Zhou, "Recent measurements of material constants versus temperature for langatate, langanite, and langasite," in *Proc. 2000 IEEE Int. Frequency Control Symp.*, pp. 200–205.

[8] E. Chilla, C. M. Flannery, H.-J. Fröhlich, and U. Straube, "Elastic properties of langasite-type crystals determined by bulk and surface acoustic waves," *J. Appl. Phys.*, vol. 90, pp. 6084–6091, Dec. 2001.

[9] H. B. Huntington, "Ultrasonic measurements on single crystals," *Phys. Rev.*, vol. 72, no. 4, pp. 321–331, 1947.

[10] E. P. Papadakis and T. P. Lerch, "Pulse superposition, pulse-echo overlap, and related techniques," in *Handbook of Elastic Properties of Solids, Liquids, and Gases*, vol. I: *Dynamic Methods for Measuring the Elastic Properties of Solids*, M. Levy, H. E. Bass, and R. R. Stern, Eds. San Diego, CA: Academic Press, 2001, pp. 39–66.

[11] J. Kosinski, A. Ballato, and Y. Lu, "A finite plate technique for the determination of piezoelectric material constants," *IEEE Trans. Ultrason. Ferroelectr. Freq. Control*, vol. 43, no. 2, pp. 280–284, Mar. 1996.

[12] P. Davulis, J. A. Kosinski, and M. Pereira da Cunha, "GaPO₄ stiffness and piezoelectric constants measurements using the combined thickness excitation and lateral field technique," in *Proc. 2006 IEEE Int. Frequency Control Symp.*, pp. 664–669.

[13] T. R. Beaucage, E. P. Beenfeldt, S. A. Speakman, W. D. Porter, E. A. Payzant, and M. Pereira da Cunha, "Comparison of high temperature crystal lattice and bulk thermal expansion measurements of LGT single crystal," in *Proc. 2006 IEEE Int. Frequency Control Symp.*, pp. 658–663.

[14] P. M. Davulis, B. T. Sturtevant, S. L. Duy, and M. Pereira da Cunha, "Revisiting LGT dielectric constants and temperature coefficients up to 120 deg. C," in *Proc. 2007 Int. Ultrasonics Symp.*, pp. 1397–1400.

[15] L. D. Doucette, M. Pereira da Cunha, and R. J. Lad, "Precise orientation of single crystals by a simple X-ray diffraction rocking curve method," *Rev. Sci. Instr.*, vol. 76, art. no. 036106, 2005.

[16] B. J. Meulendyk, M. C. Wheeler, and M. Pereira da Cunha, "Analyses and mitigation of spurious scattered signals in acoustic wave reflection measurements," *Nondestructive Testing and Evaluation Journal*, vol. 21, no. 3–4, pp. 155–169, Sep.–Dec. 2006.

[17] B. T. Sturtevant and M. Pereira da Cunha, "BAW phase velocity measurements by conventional pulse echo techniques with correction for couplant effect," in *Proc. 2006 IEEE Int. Ultrasonics Symp.*, pp. 2261–2264.

[18] V. E. Bottom, "Dielectric constants of quartz," *J. Appl. Phys.*, vol. 43, pp. 1493–1495, Apr. 1972.

[19] W. H. Press, S. A. Teukolsky, W. T. Vetterling, and B. P. Flannery, *Numerical Recipes in C++: The Art of Scientific Computing*, 2nd ed. New York: Cambridge University Press, 2002, pp. 671–675.

[20] B. J. James, "A new measurement of the basic elastic and dielectric constants of quartz," in *Proc. 1988 IEEE Int. Frequency Control Symp.*, pp. 146–154.

[21] J. Schreuer, C. Thybaut, M. Prestat, J. Stade, and E. Haussühl, "Towards an understanding of the anomalous electromechanical be-

- haviour of langasite and related compounds at high temperatures," in *Proc. 2003 IEEE Int. Ultrasonics Symp.*, pp. 196–199.
- [22] R. Fachberger, E. Riha, E. Born, and P. Pongratz, "Homogeneity of langasite and langatate wafers for acoustic wave applications," in *Proc. 2003 IEEE Int. Ultrasonics Symp.*, pp. 100–109.
- [23] D. C. Malocha and M. Pereira da Cunha, "Sensitivity analysis for extraction of material constants for trigonal crystal classes," in *Proc. 2001 IEEE Int. Frequency Control Symp.*, pp. 291–295.
- [24] D. K. Mak, "Couplant correction for ultrasonic velocity measurements," *Brit. J. NDT*, vol. 33, pp. 344–346, Jul. 1991.
- [25] D. K. Mak, "Ultrasonic phase velocity measurement incorporating couplant correction," *Brit. J. NDT*, vol. 35, pp. 443–449, Aug. 1993.
- [26] Corning Incorporated (May 2008), "HPFS fused silica standard grade specifications." [Online]. Available: http://www.corning.com/docs/specialtymaterials/pisheets/H0607_hpfs_Standard_Product-Sheet.pdf.



Blake Sturtevant (S'06) was born in Waterville, Maine, in 1981. In 2003, he received a B.A. degree in physics from Bowdoin College, Brunswick, Maine.

Mr. Sturtevant was employed for one year after college as a laboratory technician in the department of geosciences at Princeton University. Since 2004, he has been working toward the Ph.D. degree in physics at the University of Maine. His research has focused on the characterization of piezoelectric single crystals for acoustic wave applications.

Mr. Sturtevant received a SURDNA fellowship at Bowdoin College in 2002 and a Chase Distinguished Research Assistantship at the University of Maine in 2008. Since 2005, he has been a National Science Foundation IGERT trainee. He is a member of the IEEE and the American Physical Society (APS).



Peter M. Davulis (S'02) was born in Holyoke, Massachusetts, in 1983. He received his B.S. degree (summa cum laude) in electrical engineering from the University of Maine, Orono, Maine, in 2006.

Mr. Davulis has been working as a graduate assistant in the Microwave Acoustics Laboratory at the University of Maine since 2005 and is currently working toward a doctor of philosophy degree in electrical engineering at the University of

Maine. He is a teaching assistant in undergraduate electromagnetics and is researching the acoustic behavior of piezoelectric crystals for the development of acoustic wave devices.

He received a National Science Foundation Research Experience for Undergraduates Fellowship in 2005 and a University of Maine Provost Fellowship in 2006. Mr. Davulis is a member of Eta Kappa Nu and Tau Beta Pi.



Mauricio Pereira da Cunha (S'88–M'95–SM'02) was born in Brazil in 1963. He received a B.S. degree in 1985 and an M.S. degree with honors in electrical engineering in 1989 from the Escola Politécnica, Universidade de São Paulo. His master's thesis title is "Design and Implementation of a 70 MHz SAW Convolver." He received the Ph.D. degree, Dean's Honor List, from McGill University, Montreal, PQ, Canada, in electrical engineering in 1994. His Ph.D. dissertation title is "SAW Propagation and Device Modeling on Arbitrarily Oriented Substrates."

Mauricio has worked with the Microwave Devices R&D Group at Nippon Electric Company (NEC), Tokyo, Japan; Laboratório de Microeletrônica, Escola Politécnica, Department of Electrical Engineering, Universidade de São Paulo, Brazil; McGill University, Montreal, PQ, Canada; and SAWTEK Inc., Orlando, FL. He passed a sabbatical year at the University of Central Florida, Consortium for Applied Acoustoelectronic Technology (CAAT), Orlando, FL, where he worked in cooperation with Piezotechnology Inc., on the characterization of new piezoelectric materials, namely, langatate, langanite, and langasite, and with bulk and surface acoustic wave devices. Mauricio was a professor in the Department of Electronic Engineering, Universidade de São Paulo until he joined the Department of Electrical and Computer Engineering at the University of Maine in 2001, where he presently holds the position of associate professor.

Dr. Pereira da Cunha is a member of the IEEE, Sigma Xi, and of the Brazilian Microwave Society (SBMO). He was elected to serve on the SBMO Administrative Committee from 1996 to 1999. He is a reviewer and an associate editor for the *IEEE Transactions on Ultrasonics, Ferroelectrics, and Frequency Control (UFFC)*, and he has been a member of the IEEE International Ultrasonics Symposium Technical Program Committee since 1997. He has served on the UFFC-Society Administrative Committee from 2002 to 2004, served as Technical Program Committee chair for the IEEE 2007 Ultrasonics Symposium, New York, NY, and is presently the vice-chair for Ultrasonics. He has more than 140 journal, conference, and presentations in the area of microwave acoustic propagation, acoustic wave material properties, bulk and surface acoustic wave modeling and devices, and sensors.